

1 Background

Classical molecular dynamics simulations were performed to analyze the interface formed between various aqueous salt solutions and carbontetrachloride. Three salt solutions were simulated, as well as a reference system consisting of neat water for comparison to previous computational efforts.^{1–6} The salts used in the simulations were NaCl, NaNO₃, and Na₂SO₄. These were chosen to compare to the experimental SFG results, and to supplement those experiments with additional molecular-level information. Analyses were performed on the simulation data to extract ionic and molecular density data, information about water coordination near to the interface, and water orientation data from order parameter analysis. The analyses are similar to, and logical extensions of previous computational work done on aqueous salt systems.

1.1 Density Profiles

Density histograms of simulated interfaces have been used in previous publications to show ionic and molecular distribution behavior in various systems.^{2,4,6–11} In this work the density profile of water through the interface is fitted to a hyperbolic tangent function^{10,12} as shown below:

$$\rho(z) = \frac{1}{2}(\rho_1 + \rho_2) - \frac{1}{2}(\rho_1 - \rho_2) \tanh\left(\frac{z - z_0}{d}\right) \quad (1)$$

Equation (1) relates the interfacial density, ρ , as a function of position, z , along a given system axis, to the densities of the phase on either side of the location of the Gibb's dividing surface, z_0 . The bulk density ρ_1 and the density within the second phase, ρ_2 are fitted. The interfacial width, d , is related to the “90-10” thickness of the interface by:

$$t = 2.197d \quad (2)$$

These measures of interfacial thickness provide a means of comparing the depths to which the water phase is affected by ions located at the interface. The density distributions of the salts depict concentration and depletion phenomena throughout the interfacial region, and also serve to illustrate ionic affinity within this region. Previous work has been performed on the air-water interface with various ions introduced, showing varying levels of interfacial affinity, with the more polar ions being the most interfacially active. We present the density distribution results below for the neat-H₂O and salt solutions interfaced with an organic CCl₄ phase.

1.2 Molecular Orientation

Several methods have been used previously to show molecular orientation profiles of water molecules throughout simulated interfacial regions.⁷ In this work we have chosen to compute the orientation of water using two vectors that fully describe the orientation in space given the locations of the three atoms comprising

the molecule. The molecular bisector, a vector that points along the axis of symmetry of the water molecule from the hydrogen-end to the oxygen, provides directional orientation of the molecule in an intuitive way. A second vector, what is referred to here as the molecular normal vector, is established as the vector pointing normal to the plane formed by the three atoms of the water molecule and establishes the “tilt” of the molecule. Analyzing the angle made between these two vectors and a given space-fixed axis (the long axis of the system) is a means of finding the absolute orientation of waters within these simulated systems as illustrated in figure 1. The angle between the molecular bisector and the system Z -axis will hereafter be referred to as θ , and the molecular normal vector as ϕ . The analysis in this work reports the cosines of these two angles, and because of the symmetry of the water molecule where the hydrogens are not uniquely identified, the cosines of the two angles are limited as follows: $-1 \leq \cos(\theta) \leq 1$ and $0 \leq \cos(\phi) \leq 1$. We report here two-dimensional histograms showing the orientation profiles of θ and ϕ as functions of the distance from the Gibbs dividing surface of the interface, as found from the fitting in our density profile analyses.

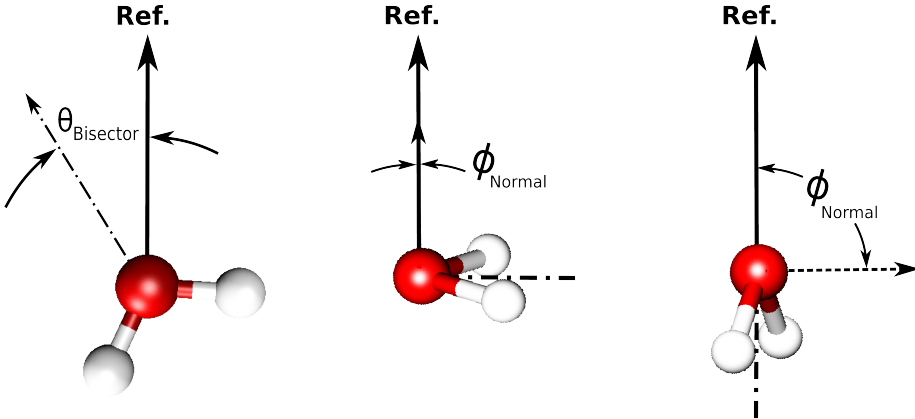


Figure. 1 — Angles used to define molecular orientation. The system reference axis (i.e. the system Z -axis) is that which is perpendicular to the plane of the aqueous-organic interface, and points out from the aqueous phase into the organic one. The molecular bisector vector points from the hydrogen-end of the water to the oxygen end, and orients along the axis of symmetry. The angle it forms with the reference axis is either aligned or anti-aligned such that $-1 \leq \cos(\theta) \leq 1$. The angle formed between the vector normal to the molecular plane (formed by the three water atoms) and the reference-axis orients the “twist” of the molecule such that $0 \leq \cos(\phi) \leq 1$, where the water molecular plane is either laying flat on the interface ($\cos(\phi) = 1$) or it the water is perpendicular to the interface ($\cos(\phi) = 0$).

1.3 Computational SFG

A difficult challenge for experimental surface studies is in understanding the vibrational spectroscopy of liquid water. Hydrogen bonding between water molecules causes intermolecular and intramolecular couplings.

Simulations provide the analytical capacity to relate the broad lineshapes, and the often difficultly assessed impact of hydrogen bonding as a function of OH vibrational frequency, to microscopic geometries, forces, and environments. In this work we compute the SFG spectra of the interface between the salt solutions and an organic phase to qualify the conclusions of a previous experimental work by our group¹³ and to elucidate some of the microscopic phenomena that lead to spectroscopic signatures.

The computational method used in this work is based on that of Morita and Hynes¹⁴ as outlined in a previous study by this group utilizing the same technique.¹⁵ The computational SFG technique has been improved in more recent studies by Morita et al,^{16,17} and with other enhanced water models. The technique used in this work has been established to recreate the qualities of the experimental spectra to a sufficient degree such that we may still draw qualified conclusions about lineshape and intensity. The most dramatic short-coming of the current technique is that of reproducing the lower-frequency features of the SFG spectra below the 3200 cm^{-1} region. However, our present analysis is concerned primarily with the overall intensity and response, and thus we still draw qualitative conclusions based on our computed results, and utilize the simpler computational methods from our previous works.

2 Computational Setup

The molecular dynamics methods used in this work are similar to those from our previous computational efforts with some modifications described below.^{1,2,4} Simulations were carried out using the Amber 9 software package. The polarizable molecular model parameters are taken from previous works on similar systems.^{7,18–21} The polarizable POL3 model was used for water molecules.²² Fully polarizable models have been used in previous interface simulation studies because they are known to more accurately reproduce interfacial structure and free energy profiles.^{23–26}

A total of 4 systems were simulated consisting of aqueous salt and CCl₄ phases. A slab geometry was used to produce two interface regions, the analyses of which were averaged.¹ The organic region was formed in a box 30- Å on a side with 169 CCl₄ molecules to reproduce standard temperature density of 1.59- $\frac{g}{mL}$. The aqueous region was formed in a box 30x30x60- Å , with the long axis labeled the z-axis. The number of water molecules and ions varied for each system in order to reproduce a density of 1.2-M. The specific populations of each molecule are listed in table 2. The organic and aqueous boxes were then joined to form a system 90- Å long with interface areas of 30x30- Å .

System	H ₂ O	Cation	Anion
Neat Water	1800	0	0
NaCl	1759	40	40
NaNO ₃	1732	40	40
Na ₂ SO ₄	1740	86	43

Table 1 — Aqueous molecule and ion numbers. Listed are the populations of each component for the 4 simulated aqueous phases. All systems were simulated at near 1.2-M salt concentrations.

The water, salts, and CCl₄ were each randomly packed into their respective boxes with a minimum packing distance of 2.4- Å . After joining the aqueous and organic phases and forming the two interfaces, the total system was energy minimized using a conjugate gradient method. Following minimization, the system was equilibrated at a constant temperature of 298-K with weak coupling to a heat bath for a period of 10-ns, using a simulation timestep of 1.0-fs. A non-bonded potential cutoff of 9.0- Å was used. Following equilibration the system was simulated with the same parameters for a further 10-ns with atomic position data recorded every 50-fs. This resulted in a total of 200,000 snapshots which were used in the data analysis.

3 Component Densities

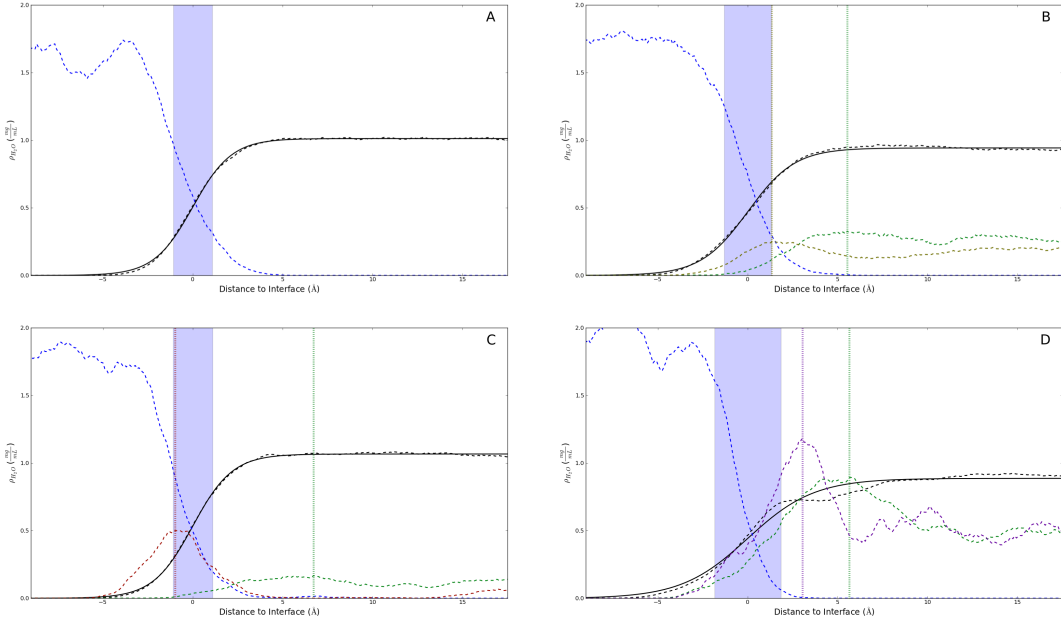


Figure. 2 — Aqueous salt and CCl_4 density profiles. The gibbs dividing surface location, z_0 , were designated as the 0.0 \AA location, and all lineshapes are plotted as distances to the gibbs interface. Neat- H_2O (A), NaCl (B), NaNO_3 (C), and Na_2SO_4 (D) salt-system densities are plotted with the water-oxygen density (dashed black) and the corresponding fitted lineshape (solid black). Each interfacial width, d , is designated as a highlighted blue region of width d centered about z_0 . The CCl_4 (dashed blue), Na^+ cation (dashed green) and respective anion densities are also shown for each system. The scaling of the cation (10x) and anion (5x) densities was used to clarify their peak and trough locations. The maxima of the ionic components are marked with dashed vertical lines of the same colors to show relative component locations within the interfacial region.

The component density profiles of each system were calculated to study the effects of adding salts and to find deviations from the neat- $\text{H}_2\text{O}/\text{CCl}_4$ system. The water density profile of each system was fitted to a hyperbolic tangent (Eq. 1), and the all the density profiles were plotted as distances from each of the gibbs dividing surface locations, z_0 . The resulting plots are shown in figure 2 with letter labels that will be used to refer to the systems. z_0 of each system was shifted to a location of 0.0 \AA , and the interfacial thickness, d , is visualized by a blue shaded region of the respective thickness centered about z_0 . The widths of the interfacial regions for the neat- H_2O (A), NaCl (B), NaNO_3 (C), and Na_2SO_4 (D) systems are 2.16 , 2.62 , 2.20 , and 3.69 \AA respectively. In each of the salt solutions, the peak in the anionic density profile occurs closer to the CCl_4 phase than the corresponding cationic peak. Various parameters of interest such as the

interfacial thicknesses, ionic component locations, and relative distances between the peaks of the ion profiles are collected in table 2.

System	<i>d</i>	Anion	Cation	Anion-Cation Distance
Neat-H ₂ O	2.16	-	-	-
NaCl	2.62	1.33	5.53	4.20
NaNO ₃	2.20	-0.99	6.71	7.70
Na ₂ SO ₄	3.69	3.04	5.64	2.60

Table 2 — Aqueous salt system density parameters. Interfacial widths, *d*, and the locations of the maxima of the density profiles for each ionic component are listed for the simulated salt systems. The relative distances between the anion and cation density peak locations are listed to show how the different anions affect the relative location of their cationic counterions.

The oscillations in the surface density profiles of water and the adjoining organic liquid phase have been noted previously and attributed to thermal capillary waves on a larger length-scale than the simulated system size.²⁷ The same work also made note that the interfacial thickness is size-dependent on the interfacial surface area. Increasing the surface area dimensions should cause an increase in the interfacial width. Two works on the water-CCl₄ surface offer direct comparison of this.^{2,27} In comparing the interfacial widths, there is an increase in width as the system cross-sectional area is increased. This phenomenon implies that care must be taken when making quantitative comparisons between simulation studies.

System A is the acting benchmark and has been simulated previously by various groups. Deviations in width of the interface from the pure-water system can be attributed to the added ions in the solution. In comparing the three salt solutions, any differences in those systems are anionic in nature because the cation of each system was kept the same. System B is the simplest of the three salts with a monatomic and monovalent anion. The peak of the anion density profile is within the aqueous phase and is found on the aqueous-side of the interfacial width, *d*. The location of the cation density peak is, as mentioned above, deeper into the aqueous phase than the anion by over 4 Å. This layering of ions within the aqueous phase is attributed to the break in the anisotropy of the field of the bulk region upon introduction of the second (organic) phase. The more polarizable and negatively charged anions move towards the interface to effectively screen the charge of the second phase and the more highly ordered water structure. The counterions then are drawn towards the negative charge built up by the anions to create the second ion density peak. The overall shape of the water profile in system B is relatively unaffected as the bulk water density is unchanged, and the width of the interface is increased by 18% from that of system A.

System C introduces the monovalent, polyatomic nitrate anion. The location preference of nitrate is a contentious subject that has been studied much in recent years. Experimental works have been performed using a few surface-sensitive techniques. One work used sum frequency generation (SFG), which detected structural changes in the hydrogen-bonding network in the presence of the anion that affect the SFG signal intensity from the interface, but could not create the anion density profile²⁸. The same work found SFG

intensity enhancement for hydrogen-bonded water following a trend of $\text{H}_2\text{SO}_4 \geq \text{HCl} > \text{HNO}_3$. Strengthening of the interfacial hydrogen-bonding structure of water would allow it to further penetrate into a second phase, thus widening the interface region, and enhancing the SFG intensity from the interface for hydrogen-bonded species. We find the same trend when comparing interfacial widths from our simulations. In the case of the nitrate anion location, however, the SFG studies stopped short of reporting a concentration profile. A recent X-ray photoemission spectroscopy study was performed to specifically determine the nitrate concentration profile for the water-vapor interface, and reported the current differences of opinion between recent experiment and simulation.²⁹ The XPS results reported a surface depletion of the nitrate anion relative to the bulk, similar to previous MD simulations of the same systems. Other works find similar nitrate surface depletions,³⁰ but were performed on the liquid-vapor interface, and help to contrast the effect of the presence of an organic phase as in the present work. We find a surface enhancement of the nitrate anion located far to the organic side of the interface. The nitrate density peak is located the furthest out from the aqueous phase of the three salt systems. The location of the sodium cation peak is a significant distance further into the bulk from the anion than either of systems B and D. Such surface location and enhancement of the nitrate ion suggests a very strong interaction with the interface waters, breaking the hydrogen-bonding network near to the organic phase, and also strongly screening the field of the CCl_4 molecules from the interface. This accounts for the narrower interfacial width as the water can no longer extend a bonded network into the organic phase. However, as the water is strongly interacting with the nitrate and effectively screening the surface charge from the bulk, the cation is less attracted to the interface and the ionic double-layer is widened. Xu, et al, studied this phenomena finding a lack of ion-pairing of various nitrates at the air-water interface.³¹ They found that solvation from an abundance of water at the interface weakens coulombic forces between ions, leading to greater cation-anion separation. They concluded that the surface nitrate is dehydrated, and the water provides adequate shielding of the ionic coulombic interactions. It is reasonable to assume that this same effect may cause the greater cation-anion separation at the interface of system C, even in the presence of the organic phase.

The widest interface is that of the NaSO_4 solution in system D, indicating that the SO_4^{2-} ions act to affect the hydrogen bonding network between the surface waters. The location of the sulfate density enhancement is the furthest into the aqueous bulk of the three anions, and the divalent and highly polarizable nature of the anion appears to attract the counterion closest for the narrowest sub-surface ionic double-layer. This attraction is likely coulombic, and the charge screening that separates the ion pairs in system C is not present in system D. Although the greatest concentration enhancement is further into the bulk region, seemingly outside the region designated by the width, the water network is still greatly enhanced. This has been verified by an increase in SFG response of the surface waters relative to the neat-water system in a recent work by this group¹³

Most of the recent studies on ion concentration near water interfaces have noted that large and polarizable ions will concentrate at the surface,^{8,25,32,33} while small non-polarizable ion tend to be repelled. The surface enhancement calculated from molecular dynamics, however, portrays the lower bound of the actual

effect because of the reduced polarizability values used in simulations to avoid the so-called “polarization catastrophe.” The enhancement of surface anions is also believed to be the cause of the subsurface cation density increase. The counterions are attracted to the concentrations of anions at the surface, which are in turn stabilized by the increased polarization of the water due to the distorted interfacial electric field. The affinity for the surface follows the trend of surface tension increments, $\frac{d\gamma}{dm_2}$, where $\text{Na}_2\text{SO}_4 > \text{NaCl} > \text{NaNO}_3$.³² This also follows the hoffmeister series trend for anions found to be the most “structure-making”, and they are found to be enhanced further into the interface.

4 Water Orientation

The orientation of water within the aqueous/organic interface of the system was defined using the angles formed by molecular axes and the fixed reference axis of the system (perpendicular to the interfacial plane). The two molecular axes used are the water bisector, pointing from the hydrogen side to the oxygen, and the vector normal to the plane formed by the three atoms of the water molecule, as depicted in figure 1. Figure 3 shows the angle profiles of both the molecular bisector and the molecular plane normal of water molecules relative to the system reference axis at various depths into the aqueous phase. Darker red regions of the plots indicate higher orientational populations, while homogeneous coloring across the angle range indicates orientational isotropy.

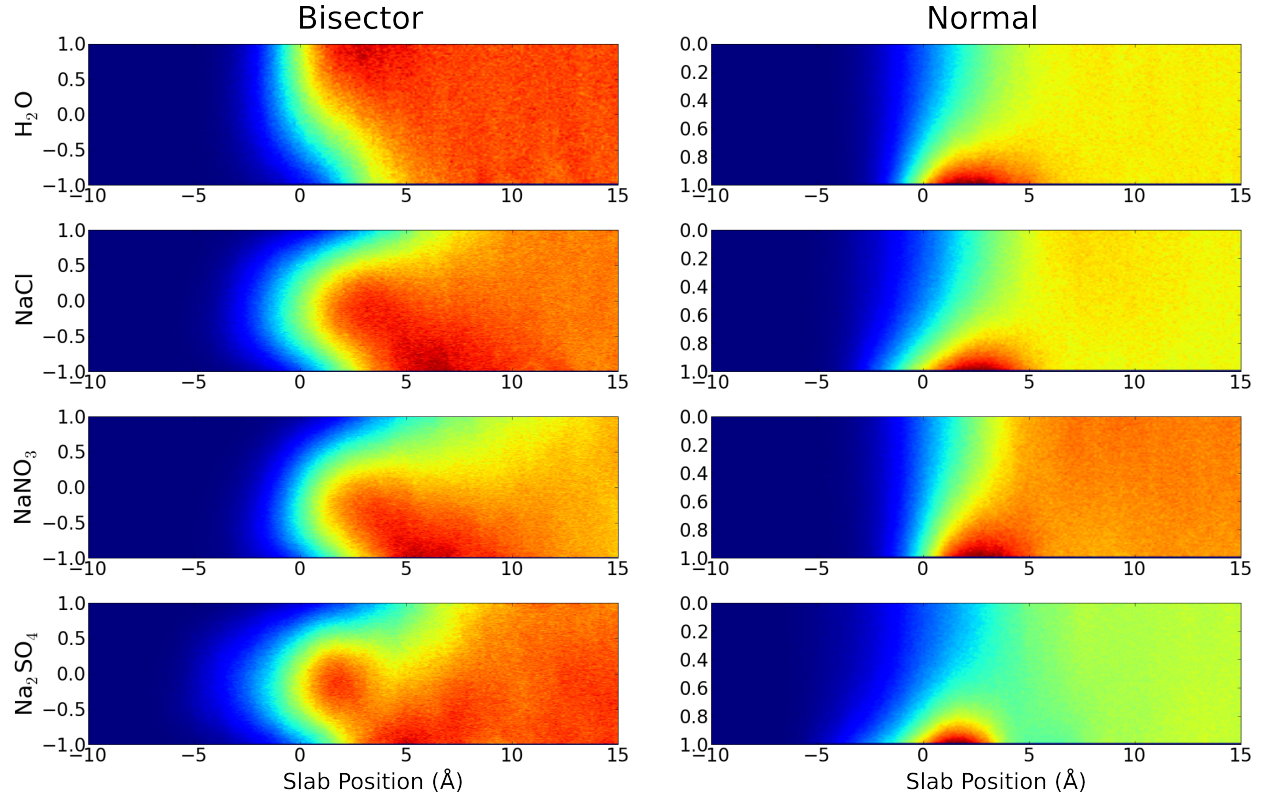


Figure. 3 — Orientation profiles of interfacial water molecules. Two profiles were developed for characterizing interfacial water orientation based on the bisector and molecular normal vector angles formed with the system references axis (see Figure 1). Each profile shows the water population for each cosine of the respective angle as a function of distance to the Gibbs dividing surface (located at 0.0). The profiles in the left column are of the bisector vector, and those on the right are of the molecular normal vector. Neat-H₂O, NaCl, NaNO₃, and Na₂SO₄ system profiles are ordered from the top to bottom row, respectively.

Previous studies have provided a detailed overview of water orientation at the interface with both air and organic phases.^{2,10,13,34,35} The topmost water layers are highly ordered because of their contact with the organic phase, and it has been suggested that ordering of both the organic and water molecules would lead to a field across the boundary of the interface.^{2,13} This can influence charged species, and the ordering and orientation of the H-bond network. Our recent experimental SFG results suggest that the accumulation of charged ions leads to a field-screening that affects the orientation of waters in the topmost layers. This is complemented by the results of the current study.

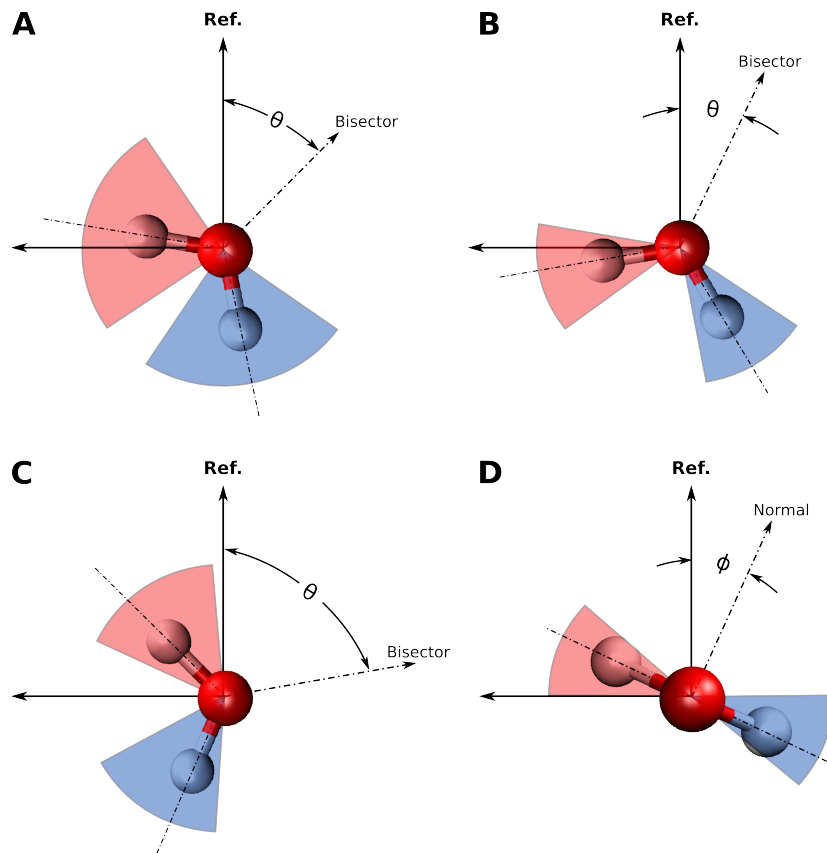


Figure. 4 — Depictions of possible orientations for different ranges of the bisector-reference angle θ . A range of $0 < \cos(\theta) < 1$ ($0^\circ < \theta < 90^\circ$ - left figure) suggests that one of the OH-bonds will always point into the aqueous phase, and the other will straddle the plane of the interface. In the range $-0.5 < \cos(\theta) < 0.5$ ($60^\circ < \theta < 120^\circ$ - center figure) one OH-bond will always point out of the aqueous phase, and the other will always remain pointing in towards the water bulk. The molecular normal angle, ϕ , has a narrow range for interfacial waters in all of the systems spanning approx. $0.7 < \cos(\theta) < 1.0$ (right). The range of ϕ keeps the topmost waters lying mostly flat on the interface, but with a narrow range of twist with OH-bonds pointing both into, and out of the interface.

In the left column of figure 3 are the bisector orientation profiles for each of the systems. The far-left dark-blue regions of the plots show the CCl_4 bulk near to the interface where few or no waters are found. The GDS is located at a depth of 0.0 Å . To the far right in the water bulk, the flat, uniformly-colored profile represents the expected isotropic orientation of the waters. The regions of interest lie around the GDS within the interface. The top bisector profile is that of the neat- H_2O system, and it shows a transition in the profile beginning just above the GDS and extending up to 5 Å into the aqueous side, at which point the profile becomes orientationally isotropic. At the GDS most of the waters are oriented between $0.0 < \cos(\theta) < 1.0$, indicating a range of orientation as depicted in figure 4a. In this range one of the OH-bonds points into the aqueous side, and the other straddles the interfacial plane with a slight affinity towards the organic CCl_4 phase. Just under the surface, between 2-4 Å into the neat- H_2O phase, a dark-red region spanning approx. $0.7 < \cos(\theta) < 1.0$ appears. This narrow orientational range is depicted in figure 4b, and is similar to the waters in the topmost aqueous layer nearer to the GDS, but limited such that both OH bonds point into the H_2O side, with one of them only straddling the interfacial plane with a tendency to point into the H_2O phase.

The neat- H_2O bisector orientational profile is comparable to previous simulations of the same neat- H_2O reference system. Using different simulation parameters for the same neat- $\text{H}_2\text{O} / \text{CCl}_4$ system, Wick and Dang found the free-OH to point slightly into the CCl_4 phase at the GDS with an angle of $\cos(\theta)_{free-OH} \approx 0.4$. This corresponds to $\cos(\theta)_{bisector} \approx 0.5$ in the this work's angle definition. Similarly, deeper into the surface the angle profile diminishes such that $\cos(\theta_{free-OH}) \approx 0.0$ within 5 Å of the GDS, corresponding to $\cos(\theta_{bisector}) \approx 0.8$ in the current scheme. Those results agree with this work's neat- H_2O profile, further complementing the experimental SFG conclusions performed on the same systems.^{13,36}

Bisector angle profiles for the salt systems show different behavior than that of the reference neat- H_2O system. The profiles of the salt systems at the GDS all center about the $\cos(\theta) = 0$ region, with a range of approx. $-0.5 < \cos(\theta) < 0.5$. This indicates a straddling water molecule with the orientational range depicted in figure 4c. The water in that range is clearly oriented such that one OH-bond always points out of the aqueous phase into the CCl_4 , and the other always points in to the water bulk. The OH-bond that would straddle the interface in the neat-water system points out of the interface with a greater angle. This orientation, centered about $\cos(\theta) \approx 0$, extends into the water phase up to 3 Å , at which point the profile shifts to the darker region near $-0.7 < \cos(\theta) < -1$. The sub-surface region of the profile between 4-7 Å in each system corresponds to a flip of the water orientation, as referred to in a recent SFG study as a “flip-flop” model where water orients to counteract the field of charged species at interfaces.⁷ The cation density enhancement in each salt system is within the region of 5-7 Å below the GDS. The waters may be orienting with the negatively charged oxygen end towards those cations, and with the field established by the ion double-layer within the interface. In each of the salt bisector profiles there is a clear depletion of waters oriented towards $\cos(\theta) = 1$ suggesting that alignment of the bisector with the reference axis is not preferred. The effect is most pronounced in the Na_2SO_4 system where the distance between counterion density enhancements is smallest, and the transition in the bisector profile is the most abrupt, changing

from a profile mostly in the range of $0.5 < \cos(\theta) < -1.0$ to isotropic orientation quickly near 8 Å into the aqueous phase. The NaNO₃ system bisector profile shows the effect furthest into the water bulk, extending almost to 13 Å. Counterion density enhancement is most separated in NaNO₃, however, and most of the orientational affinity for $0.5 < \cos(\theta) < -1.0$ occurs within the first 10 Å of the surface. The bisector profile of the NaCl system is broadest with $0.7 < \cos(\theta) < -1.0$ starting near the GDS. Also, orientational isotropy is shallowest in the NaCl system starting near 7 Å into the surface.

It appears that the field established by the anion-cation pairing within the interface affects the depth to which waters are oriented before the bulk isotropic profile begins. Also, the range of orientations beneath the surface is dependent on the properties of the anion. The weakly polarizable Cl⁻ anion does not restrict the orientational range as much as the more polarizable NO₃⁻ and SO₄²⁻. Anions also appear to control the depth to which the water orientation is felt, with the most surface-active NO₃⁻ anion causing the deepest effect. SO₄²⁻ anion shows the strongest restriction on the range of bisector angles, and the sharpest orientational transition to the bulk, which may be attributed to the higher charge of the anion, and thus the stronger field established between the counterions in the system.

The molecular plane normal in the right column of figure 1 is clearly centered about the flatter orientations with $0.7 < \cos(\theta) < 1.0$. This profile suggests that the water lies flat on the interface with a twist of up to 45°. Molecular normal orientation profiles are very similar across the systems investigated, with each profile showing an affinity for the flat orientation starting just before the GDS, and extending as deep as 7 Å in the water and NaCl systems, and between 3-4 Å in the NaNO₃ and Na₂SO₄ polyatomic salt systems.

5 Calculated Sum-Frequency Spectra

One of the aims of this simulation study is to complement our group's previous experimental SFG work.¹³ The varied set of anions and their affect on the $\text{CCl}_4\text{-H}_2\text{O}$ interface is linked from theory to empirical data through the connection of computed SFG spectra. The computed SFG spectra for each system are presented in figure 5 along with the experimental spectra from our previous work with these same salt solutions.¹³ On first look, the overall intensities and lineshapes follow remarkably similar trends as in the experimental systems. The key features of the $\text{CCl}_4\text{-H}_2\text{O}$ interfacial spectra are the diminished intensities below 3400 cm^{-1} as compared to previous liquid-air works, and the dominant "free-oh" peak near 3660 cm^{-1} .

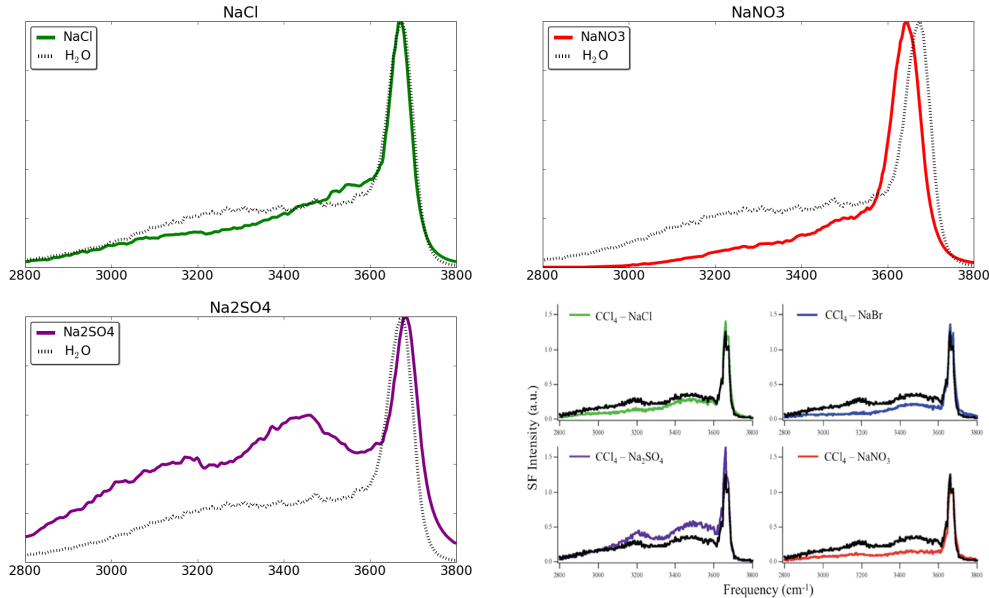


Figure. 5 — Vibrational SFG spectra of the water-OH stretching region for each interfacial aqueous-salt/ CCl_4 system. The water/ CCl_4 interface spectrum (black-dashed line) is provided on the plot for each of the simulated systems for reference. The bottom-right figure is a reproduction of the experimental spectra from McFearin et al to show the intensity and lineshape trends found previously for these systems.¹³

The reference $\text{CCl}_4\text{-H}_2\text{O}$ spectrum reproduces well the lineshape from experiment, but lacks the definition of the two peaks found near 3250 and 3450 cm^{-1} . These lower-frequency features have been attributed to the different H-bonding varieties of water that make up the more highly-coordinated, tetrahedral environments found deeper into the aqueous bulk. We have found similar trouble in reproducing the lower-frequency peaks near 3200 cm^{-1} , and attribute the slight differences in the lineshape to similar problems.⁴ However,

the lineshape is otherwise quite similar to that of the experiment, and warrants further comparison, and suggests that the methods are sound, and justified for this study.

For monovalent ions at the CCl₄-H₂O interface, the behavior is completely different than for the air-H₂O systems. Previous works found concentrations of monovalent anions to be lower at the CCl₄-H₂O interface than at the air-liquid one.³⁷ However, larger and more polarizable anions were found to be less solvated than smaller ones such as Cl⁻, and more surface active. I⁻, for instance, has more contact with the CCl₄ phase because of a more exposed surface area and higher polarizability, resulting in repulsion of the CCl₄, and a wider aqueous interface. The exposure to the CCl₄ phase decreases the anion concentration relative to the air-water interface, yet a very prominent density peak remains at the interface for those larger and polarizable ions. The presence of anions at the interface results in a “field-screening” that decreases the effect of the changing interfacial field further into the aqueous bulk. Water molecules found below the surface, those giving rise to the lower-frequency 3500 cm⁻¹ OH-stretch features, are thus less oriented by the field and their SFG contribution is decreased. Both the monovalent anions, Cl⁻ and NO₃⁻, show this effect in their SFG spectra. Comparison to the reference neat-H₂O spectrum shows that the added presence of the surface-active anions decreases the lower-frequency intensities, as found in the experimental study. The Cl⁻ has a notably smaller decrease in the spectral intensities than the NO₃⁻ system. This expected result is most likely due to the higher preference for the surface of the larger, and more polarizable nitrate. The NO₃⁻ ion is extremely surface active, as seen in the density profile, and should thus cause the greatest “field-screening” to waters found deeper in the bulk.

The divalent and larger SO₄²⁻ anion accumulates deeper into the aqueous bulk and exhibits the lowest surface affinity of the ions studied. This is likely due to the higher charge of the anion that leads to greater solvation. The sulfate provides little or no screening of the interfacial field from the top-most water layer, and only affects the deeper waters. Lower frequency features of the water OH-spectrum spectrum are notably higher in intensity and both the 3250 and 3450 cm⁻¹ features are present, and dominate as compared to the reference water system, in both the simulated and experimental spectra.

As concluded in the previous experimental work, the monovalent anions appear to screen the deeper water molecules from the field produced by the phase change at the aqueous-organic interface. Larger and more polarizable monovalent anions have a stronger screening effect due to their increased surface affinity. The large but more highly charged divalent anion experiences greater solvation and is thus found deeper in the aqueous phase. Deeper anions do not participate as field screening agents to the same extent as their monovalent counterparts, and the result is an increase across the lower frequencies of the water OH-stretching SFG spectrum.

References

1. Hore, D. K.; Walker, D. S.; MacKinnon, L.; Richmond, G. L. *Journal of Physical Chemistry C* **2007**, *111*, 8832-8842.
2. Hore, D. K.; Walker, D. S.; Richmond, G. L. *Journal of the American Chemical Society* **2008**, *130*, 1800+.
3. Hore, D. K.; Walker, D. S.; Richmond, G. L. *Journal of the American Chemical Society* **2007**, *129*, 752-753.
4. Walker, D. S.; Hore, D. K.; Richmond, G. L. *Journal of Physical Chemistry B* **2006**, *110*, 20451-20459.
5. Walker, D. S.; Richmond, G. L. *Journal of the American Chemical Society* **2007**, *129*, 9446-9451.
6. Walker, D. S.; Moore, F. G.; Richmond, G. L. *Journal of Physical Chemistry C* **2007**, *111*, 6103-6112.
7. Chang, T.; Peterson, K.; Dang, L. *Journal of Chemical Physics* **1995**, *103*, 7502-7513.
8. Eggimann, B. L.; Siepmann, J. I. *Journal of Physical Chemistry C* **2008**, *112*, 210-218.
9. Du, H.; Liu, J.; Ozdemir, O.; Nguyen, A. V.; Miller, J. D. *Journal of Colloid and Interface Science* **2008**, *318*, 271-277.
10. Wick, C.; Dang, L. *Journal of Physical Chemistry B* **2006**, *110*, 6824-6831.
11. Petersen, P.; Saykally, R.; Mucha, M.; Jungwirth, P. *Journal of Physical Chemistry B* **2005**, *109*, 10915-10921.
12. Matsumoto, M.; Kataoka, Y. *Journal of Chemical Physics* **1988**, *88*, 3233-3245 hyperbolic tangent fitting function for water density profiles.
13. McFearin, C. L.; Richmond, G. L. *Journal of Physical Chemistry C* **2009**, *113*, 21162-21168.
14. Morita, A.; Hynes, J. *Chemical Physics* **2000**, *258*, 371-390.
15. Walker, D. S.; Richmond, G. L. *Journal of Physical Chemistry C* **2007**, *111*, 8321-8330.
16. Morita, A.; Hynes, J. *Journal of Physical Chemistry B* **2002**, *106*, 673-685.
17. Ishiyama, T.; Morita, A. *Journal of Physical Chemistry C* **2009**, *113*, 16299-16302.
18. Chang, T.; Dang, L. *Journal of Physical Chemistry B* **1997**, *101*, 10518-10526.
19. Dang, L. *Journal of Physical Chemistry B* **1999**, *103*, 8195-8200.

20. Thomas, J. L.; Roeselova, M.; Dang, L. X.; Tobias, D. J. *Journal of Physical Chemistry A* **2007**, 111(16), 3091-3098.
21. Hrobarik, T.; Vrbka, L.; Jungwirth, P. *Biophysical Chemistry* **2006**, 124, 238-242.
22. Caldwell, J. W.; Kollman, P. A. *J. Phys. Chem.* **1995**, 99, 6208-6219.
23. Rivera, J. L.; Starr, F. W.; Paricaud, P.; Cummings, P. T. *Journal of Chemical Physics* **2006**, 125.,
24. Wick, C. D.; Kuo, I.-F. W.; Mundy, C. J.; Dang, L. X. *Journal of Chemical Theory and Computation* **2007**, 3, 2002-2010.
25. Petersen, P.; Saykally, R. *Journal of the American Chemical Society* **2005**, 127, 15446-15452.
26. Dang, L. *Journal of Physical Chemistry B* **1998**, 102, 620-624.
27. Chang, T.; Dang, L. *Journal of Chemical Physics* **1996**, 104, 6772-6783.
28. Schnitzer, C.; Baldelli, S.; Shultz, M. *Journal of Physical Chemistry B* **2000**, 104, 585-590.
29. Brown, M. A.; Winter, B.; Faubel, M.; Hemminger, J. C. *Journal of the American Chemical Society* **2009**, 131, 8354+.
30. Otten, D. E.; Petersen, P. B.; Saykally, R. J. *Chemical Physics Letters* **2007**, 449, 261-265.
31. Xu, M.; Tang, C. Y.; Jubb, A. M.; Chen, X.; Allen, H. C. *Journal of Physical Chemistry C* **2009**, 113, 2082-2087.
32. Pegram, L. M.; Record, Jr., M. T. *Proceedings Of The National Academy Of Sciences Of The United States Of America* **2006**, 103, 14278-14281.
33. Sloutskin, E.; Baumert, J.; Ocko, B. M.; Kuzmenko, I.; Checco, A.; Tamam, L.; Ofer, E.; Gog, T.; Gang, O.; Deutsch, M. *Journal of Chemical Physics* **2007**, 126.,
34. Fan, Y.; Chen, X.; Yang, L.; Cremer, P. S.; Gao, Y. Q. *Journal of Physical Chemistry B* **2009**, 113, 11672-11679.
35. Wick, C. D.; Dang, L. X. *Chemical Physics Letters* **2008**, 458, 1-5.
36. Scatena, L.; Richmond, G. *JOURNAL OF PHYSICAL CHEMISTRY B* **2001**, 105, 11240-11250.
Nihonyanagi, S.; Yamaguchi, S.; Tahara, T. *Journal of Chemical Physics* **2009**, 130.,
37. Wick, C.; Dang, L. X. *Journal of Chemical Physics* **2007**, 126.,